Analyst

PAPER

Cite this: *Analyst*, 2017, **142**, 1974

Label-free detection of DNA hybridization with a compact LSPR-based fiber-optic sensor†

Savannah Kaye,‡[a] Zheng Zeng,‡[b] Mollye Sanders,[a] Krishnan Chittur,[c,d] Paula M. Koelle,[d] Robert Lindquist,[a] Upender Manne,[e] Yongbin Lin*[a] and Jianjun Wei *[b]

Received 11th February 2017,
Accepted 21st April 2017

DOI: 10.1039/c7an00249a

rsc.li/analyst

A miniaturized, robust, localized surface plasmon resonance (LSPR)-coupled fiber-optic (FO) nanoprobe providing an integrated and portable solution for detection of DNA hybridization and measurement of DNA concentrations has been demonstrated. The FO nanoprobe was created by constructing arrays of metallic nanostructures on the end facets of optical fibers utilizing nanofabrication technologies, including electron beam lithography and lift-off processes. The LSPR-FO nanoprobe device offers real-time, label-free, and low-sample-volume quantification of single-strand DNA in water with high sensitivity and selectivity, achieving a limit of detection around 10 fM. These results demonstrate the feasibility of the LSPR-FO nanoprobe device as a compact and low-cost biosensor for detection of short-strand DNA.

Introduction

The development of highly selective and sensitive DNA hybridization-based detection technology has been propelled by demands in the fields of genetic disease diagnostics, molecular medicine, and forensics. However, small sample volumes, low analyte concentrations, and high cost present a challenge to current nucleotide sensors.[1] Furthermore, to support medical diagnosis and health monitoring in remote and resource-poor areas, highly sensitive and portable biosensor systems are needed to monitor multiple physiological parameters in humans to predict, access, and solve health-related problems. The biosensors used under these conditions must be small and robust, use small amounts of reagents, and have few processing steps.

Owing to its potential to realize an ultra-compact and high-sensitivity device, surface plasmon resonance (SPR) of noble metallic nanostructures has been explored for biosensing applications based on its extraordinary optical properties.[2–4] A collective oscillation of the conductive electrons within the surfaces of noble metal nanostructures can be excited by electromagnetic waves, giving rise to enhanced electromagnetic fields localized at the dielectric/metal interface. The resonance wavelength of SPR is dependent on the dielectric environment, which has been explored as the working principle for chemical and biological sensing. There are two types of plasmonic excitation, propagating SPR (P-SPR) and localized SPR (LSPR).[5] P-SPR, based on a continuous metallic thin film, has been applied in chemical and biological sensing for a diverse range of fields.[6] LSPR is based on the interaction of light with nanoparticles of noble metals on a scale smaller than wavelengths of incident light.[7] Similar to P-SPR, LSPR, which is sensitive to changes in the local refractive index (RI), provides flexibility, allowing researchers to tune the resonance wavelength from the visible to the infrared region of the light spectrum by varying the shape, size, and material of the nanostructures that support the LSPR.[6–8] Another advantage of LSPR sensing is that it can be made compact and can use ultra-small amounts of agents in detection, factors that are suitable for remote health monitoring.[2]

Silica glass slides are a popular choice as substrates for biosensors based on LSPR of gold nanostructures. Nanofabrication approaches, such as electron-beam lithography (EBL),[9] focused ion beam, holographic lithography,[10] and nanosphere lithography,[11,12] have been developed to construct the metallic nanoparticles[13] on glass slides. New nanostructure configurations (*e.g.*, nanoshells,[14] dimer/trimer nanoantennas,[15,16] nanostars,[17] and nanocrescents[18]) have been investigated for enhanced performance (*e.g.*, stability and

[a]*Center for Applied Optics, University of Alabama at Huntsville, Huntsville, AL 35899, USA. E-mail: liny@uah.edu*
[b]*Department of Nanoscience, Joint School of Nanoscience and Nanoengineering, University of North Carolina at Greensboro, Greensboro, NC 27401, USA. E-mail: j_wei@uncg.edu*
[c]*Chemical and Materials Engineering, University of Alabama Huntsville, Huntsville, AL 35899, USA*
[d]*Genecapture, 601 Genome Way, Huntsville, AL 35806, USA*
[e]*Department of Pathology, University of Alabama at Birmingham, AL 35249, USA*
†Electronic supplementary information (ESI) available: Optical setup scheme, reflection spectra of the nanoprobe for reusability, FDTD simulation for magnetic field distribution. See DOI: 10.1039/c7an00249a
‡Equal contribution.

sensitivity). The measurement setup for the LSPR on glass slides typically includes an optical microscope and optical alignment apparatus. Although the phenomenon of LSPR has been recognized for being sensitive and specific in biosensing applications, traditional glass slide-based LSPR platforms have not been well accepted for practical applications beyond research laboratories, due to limitations, such as difficulties with regard to sample handling and the requirements of highly trained personnel and expensive desktop apparatus.

Research efforts have been made to overcome these limitations by coupling LSPR sensing and fiber optic (FO) technology, thus creating a new family of devices called LSPR fiber optic (LSPR-FO) sensors.[19–21] An optical fiber, an excellent waveguide for visible to infrared light, has the characteristics of small size, high mechanical strength, and flexibility. The small cross-section and large aspect ratio of the fiber provides an inherently light-coupled substrate (fiber tip) that is suited for remote, *in vivo* and *in situ* applications. Combining optical fiber tips with metallic plasmonic nanostructures, the entire biosensing system can be miniaturized and made portable for measurements outside the laboratory environment, applicable to point-of-care applications and resource-poor areas. Moreover, the LSPR-FO may provide other advantages as well, such as biocompatibility, all-optical interrogation, low-cost components, and the capacity for multichannel performance required in high-throughput screening applications. Due to the location of the metallic nanostructures on the tip of the optical fiber over the core, optical alignment between the optical fiber and the test environment is not required, thereby avoiding drawbacks associated with conventional LSPR sensors on glass slides including the use of bulky optics and high-precision mechanics, and making the LSPR-FO biosensing technology suitable for point-of-care and field applications.

In our previous study, we devised a method for fabricating metallic nanostructures on the end facets of optical fibers utilizing EBL and reactive ion etching.[22–24] Recently, we presented[25] an improved LSPR-FO nanoprobe for ultrasensitive detection of protein biomarkers. The nanoprobe is fabricated with an advanced lift-off process to transfer nanoscaled disk-like patterns from an e-beam resist layer to an Au thin film at the optical fiber tip surface, offering a low-cost solution with minimum damage to the fiber end facet. The well-aligned controllable nanodisk array at the fiber end provides additional advantages, such as stability, reusability and tunable optical properties (*vide infra*), over conventional adhered nanoparticle-based LSPR-FO sensors. Although the current fabrication method using EBL is complicated and time-consuming, for practical purposes, the high-throughput and low-cost method using nano-imprint lithography (NIL) on a fiber tip seems promising and is currently underway for the fiber-tip nanodisk array fabrication.

Motivated by the prospect of improving the sensitivity and point-of care application of DNA hybridization-based sensors, the present work is focused on the feasibility of using a miniaturized LSPR-FO nanoprobe for detection of DNA. The model DNA used for hybridization is the "ARC" probe, a DNA sequence designed to target a 16S rRNA sequence found in archaea and used to probe for archaea targets in complex mixtures.[26,27] DNA immobilization and hybridization on the LSPR-FO platform cause changes in the interfacial RI, which are monitored by reflection LSPR spectra from the LSPR-FO tip surfaces. Moreover, a numerical tool, the finite difference time domain (FDTD) method, was used to understand, qualitatively and quantitatively, the link between the optical responses and the underlying SPR mechanism by solving Maxwell's equations.[28]

Materials and methods

Materials and reagents

Single-mode optical fibers for 633 nm wavelength were purchased from Newport Corporation (F-SV). Electron beam resist (ZEP-520A), thinner (ZEP-A), developer (ZED-N50), and resist remover (ZEDMAC) were purchased from ZEON Corporation, Japan, and used without further purification. ARC probe DNA, ARC target DNA (complementary to the probe), and NEG target DNA (a control sequence) were obtained from Integrated DNA Technologies (Coralville, IA, USA). Saline–sodium phosphate–EDTA (SSPE) hybridization buffer was obtained from Genecapture (Huntsville, AL). All other solvents were purchased from Sigma and used without further purification.

Fabrication of the LSPR-FO nanoprobe

We have developed a cleanroom process for the fabrication of robust LSPR-FO nanoprobes on the flat end-facets of a single-mode optical fiber using semiconductor fabrication technologies. The microscopic cross-section and large aspect ratio of the fiber tip platform present challenges for fabricating nanoscale transducers on the fiber tip. Modifications to the standard planar fabrication technologies were made to address these challenges, especially to the resist coating process.[25] Briefly, there are 4 main technological steps: (1) deposition of positive electron beam resist (ZEP520A) on the fiber end facet with uniform thickness, using a dip and vibrate technique, (2) nano-patterning on the e-beam resist using an EBL method, (3) vacuum deposition of functional metallic materials over the e-beam resist using cleanroom thermal evaporation, and (4) nano-pattern transfer using a standard lift-off method.

These experiments were accomplished using an unmodified and low-cost single-mode optical fiber for a wavelength of 633 nm, with a core diameter of 4 μm, a cladding diameter of 125 μm, and a polymer buffer coating diameter of 250 μm. The optical fiber tip was prepared by stripping the polymer buffer layer 4 cm from the end and cleaving the fiber with a fiber cleaver, followed by cleaning with acetone and a rinse with isopropyl alcohol. A layer of 2 nm Cr acting as a conductive layer for the EBL process and an adhesive layer for Au film overlay were deposited on the fiber tip end-facet by using a vacuum sputtering system.

A simple and distinctive wet-resist coating method called "dip and vibration" was developed to process the optical fiber

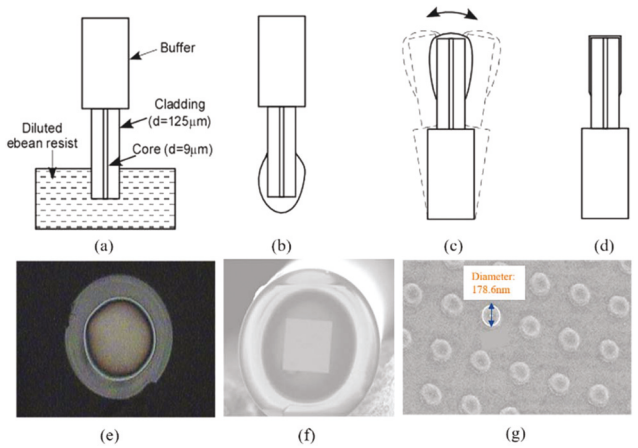

Fig. 1 Illustration of the procedure used to coat the end facets of an optical fiber with a uniform layer of electron beam resist. Panels (a) to (d) depict the nanofabrication procedure. Panel (e) is an SEM of image of resist coating on the fiber tip. Panel (f) is an SEM image of the fiber end facet after the EBL process. Panel (g) is an SEM image of the nanodot array at the tip end surface.

tip, as schematically represented in Fig. 1. The optical fiber was dipped in diluted e-beam resist (ZEP520A diluted with anisole at ratio of 1 : 3) for 10 seconds (Fig. 1a). Then it was removed from the resist (Fig. 1b) and hoisted to a vertically upward position using a Newport fiber clamp. The fiber tip was vibrated to remove excessive resist by cantilever-beam free vibration (Fig. 1c). The vibration frequency and strength were controlled by the length of the fiber tip outside of the fiber clamp and the initial displacement of the fiber tip. The thickness of the resist on the optical fiber tip depended on the ZEP dilution ratio and vibration strength. An iterative method was used to achieve the optimized resist thickness (~100 nm), which could be monitored by scanning electron microscopy (SEM). After resist coating, the fiber tip was held vertically and baked in a 120 °C oven for 60 minutes (Fig. 1d).

The EBL process based on the nano pattern generation system and a field emission scanning electron microscope was used to create a nanodot array pattern on the e-beam resist on the fiber end facet. The fiber tip was developed by dipping in resist developer (ZEP N50) for 1 minute. The fiber tip was then rinsed in deionized (DI) water and baked in a 120 °C oven for dehydration. An oxygen plasma de-scum procedure (25-Watt power for 3 minutes) was used to remove thin residual layers of photoresist areas following photoresist development.

The deposition of a 55 nm Au overlay over the patterned area was accomplished by using a standard thermal evaporation coating technique. To lift off the e-beam resist, the fiber tip was dipped in the ZEP remover for 10 minutes, followed by a 1-minute ultrasonic bath to assist the lift-off process. The fiber tip was rinsed in DI water and checked under an optical microscope to assure that the resist layer has been removed. Then the fiber tip was dipped into the Cr remover solution for 30 seconds to remove the Cr layer that was not covered by the Au nanoparticles. The fiber tip was rinsed again in DI water and baked for 10 minutes in a 120 °C oven for dehydration. Finally, the fiber tip was annealed at 530 °C for 2 minutes through an access hole on a sidewall of a high-temperature oven.

Optical measurement

The setup for characterizing the optical fiber tip LSPR sensors based on backward scattering is similar to a previous report (see Fig. S1†),[25] in which both the excitation and the LSPR scattering of light occur at the fiber distal end. A 2 × 1 fiber coupler with a coupling ratio of 50 : 50 at the wavelength of 633 nm was used to guide the light. The fabricated fiber probe was connected to the single arm of the fiber coupler by a fusion splicer. On the double-arm side of the fiber coupler, the incident light was launched from a tungsten halogen white light source (LS-1, Ocean Optics Inc., USA), and the reflected signal was routed and captured by a mini-spectrometer (Ocean Optics).

The reference spectrum was acquired without a fiber probe, and with the fiber end facet freshly cleaved. The dark spectrum was obtained by turning off the tungsten halogen light source and room light. The measured reflection spectra (M_λ) of the fiber tip sensor probe were obtained by $M_\lambda = [(S_\lambda - D_\lambda)/(R_\lambda - D_\lambda)] \times 100\%$, where S_λ is the sample intensity, D_λ is the dark intensity, and R_λ is the reference intensity at wavelength λ.

DNA strands for sensing

To demonstrate the capability of the fiber-based LSPR probe as a biosensor for detection of DNA and to establish its sensitivity and specificity, the LSPR-FO probe was functionalized with a probe DNA strand and used to detect the hybridization of complementary strands of target DNA. The DNA under study was comprised of two sets of corresponding DNA strands, ARC probe DNA and ARC target DNA obtained from Integrated DNA Technologies (Coralville, IA, USA). The ARC probe DNA, a thiolated, single stranded DNA (HS-ssDNA), was a 20-base pair oligonucleotide with the following sequence: 5′-/5ThioMC6-D/GTGCTCCCCCGCCAATTCCT-3′. The ARC target DNA, a complementary ssDNA, having a complementary nucleotide sequence as the ARC probe DNA but without the HS-(CH2)6-attachment at the 5′ end, had a sequence of 5′-AGGAATTGGCGGGGGAGCAC-3′. Each DNA oligonucleotide was 20 base pairs long. SSPE buffer solution was used for DNA hybridization. For the control experiments, another 20-base-pair DNA strand, NEG target DNA (5′-CAACCGGTTATTTTTCTACA-3′) was used. The NEG DNA sequence was not expected to bind to the probe, ARC DNA. The analytical grade solvents used for cleaning the tip were ethanol, acetone, methanol, isopropyl alcohol, and DI water.

Before starting an experiment, the sensor tip was cleaned of any impurities or other contaminants by a rinse in ethanol. A baseline wavelength was achieved if the sensor tip returned to this wavelength three times after being washed in DI water. If the tip did not return to this line, acetone and isopropyl alcohol were used to clean the tip of lingering impurities.

Monitoring the tip functionalization

ARC probe DNA was diluted to 100 μM concentration with DI water. The diluted samples were stored in a freezer at −20 °C while not being used. Several μl of the probe were added to a microcentrifuge tube clamped into place underneath the sensor tip. Once the sensor tip was placed in the DNA solution, the setup was allowed to sit for 24 hours. After this incubation, the probe sensor tip was rinsed three times with DI water and dried in air. From the displayed spectrum, a MATLAB program was used to determine the peak wavelength of the reflectance spectrum.

Detection of the target DNA and control experiments

The original ARC target DNA was diluted to 100 μM concentration with DI water. These stock solutions were then diluted with SSPE buffer to obtain twelve samples of each target ranging from concentrations of 100 μM to 1 fM. The probe tip used the corresponding target DNA for testing. First, the probe tip was placed in the smallest concentration (10 μl volume) of target for ten minutes and then rinsed three times with DI water. The reflectance spectrum was recorded, and the spectral peak was determined by the MATLAB program. The same tip, without any probe being washed off, was placed into the second lowest concentration for ten minutes. This was then rinsed three times with DI water, and the reflectance spectrum was recorded. This procedure was used through all twelve dilutions of the target DNA. Once all spectra were obtained and recorded, these could be compared to the probe spectrum before binding to determine the wavelength shift for each target DNA concentration. Numerical data were obtained from the reflectance graph produced using the SpectraSuite program from Ocean Optics Inc. (FL, USA).

The LSPR-FO probe was coated with DNA that had a specific, known sequence – designed to hybridize to target sequences from the solution with a complementary sequence. We could not, however, rule out non-specific adsorption/binding of DNA molecules from the solution to the LSPR-FO surface. We designed a sequence called "NEG" (negative) that did not have any overlap with the ARC probe DNA and which was not expected to bind to the LSPR nanoprobe. For a control experiment, the ARC probe DNA tip was submerged in the NEG target DNA at concentrations similar to the "ARC" target DNA solutions, and the LSPR reflectance spectra were recorded.

Simulation method

The numerical FDTD solutions combined with MATLAB codes were used to assess the optical response of the LSPR-FO nanoprobe, with the following simulation layout setting details. The total mesh area had a background RI of 1.0 (air) and a RI of 1.5 for the organic layer. Periodic boundary conditions (BCs) and matched layer BCs were applied along *x*-, *y*-, and *z*-boundaries of the unit cell. The indices of Au and substrates followed the data of optical constants of solids.[29] The geometry of the Au nanodots array used in the modeling was a square array with 400 nm periodicity; each nanodot had a disk-like shape with 55 nm thickness and 180 nm diameter. The relative permittivity of Au is given with the Drude–Lorentz model:

$$\varepsilon_r = \varepsilon_\infty + \sum_{n=1}^{N} \frac{x_0 G_n {\omega_{0n}}^2}{{\omega_{0n}}^2 + i\Gamma_n \omega - \omega^2}, \sum_{n=1}^{N} G_n = 1 \qquad (1)$$

where ε is the permittivity, ω_{0n} is the resonant frequency, Γ_n is the damping coefficient, ∞ means infinity, and x_0 is the permittivity at ω_0.

Results and discussion

Fabrication results and characterization

The RI sensitivity of the LSPR-FO probes for the bulk dielectric environment was in the range of 220–230 nm wavelength shift per RI unit (RIU). The fiber LSPR probe was dipped in various solvents (methanol, water, acetone, ethanol, and isopropyl alcohol). The spectra of the reflected light were recorded, and the LSPR peak wavelength was obtained using a MATLAB program to fit the best polynomial function to the experimental data. When the LSPR-FO probe was dipped in various solvents, the LSPR wavelength shifted red as the RI of the solvent increased.

Functionalization of the LSPR-FO nanoprobe

To detect the target DNA in the buffer, a biosensing strategy based on the immobilization of the probe DNA on the surface of the Au nanodisk on the fiber tip was addressed. Fig. 2 shows a schematic of the strategy. A cleaned LSPR-FO nanoprobe was first functionalized with probe DNA, which was designed to bind specifically with its complementary target DNA. The thiol end on the probe DNA molecule allowed formation of a dative bond between the Au nanodisk surface and the probe DNA, creating a stable chemical structure and a monolayer of probe DNA molecules over the Au surface by the self-assembled monolayer process. To determine the binding of the ARC probe DNA to the LSPR-FO, the sensor was cleaned in acetone and isopropyl alcohol, and a baseline spectrum was obtained in air. For functionalization, the probe was placed in an ARC probe solution for 24 hours. Then the probe tip was rinsed three times with DI water and dried in air. All the functionalization and the sensing spectra were taken in air.

The LSPR peak wavelength shift of the ARC probe functionalization step is shown in Fig. 3; there was an average wavelength shift of 8.3 ± 0.6 nm from the baseline for the six

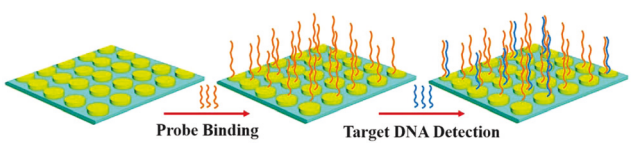

Fig. 2 Schematic representation of the miniaturized LSPR-FO nanoprobe, with the biofunctionalization methodology based on the covalent coupling of the probe DNA to the nanodisk surface and the subsequent detection of target DNA.

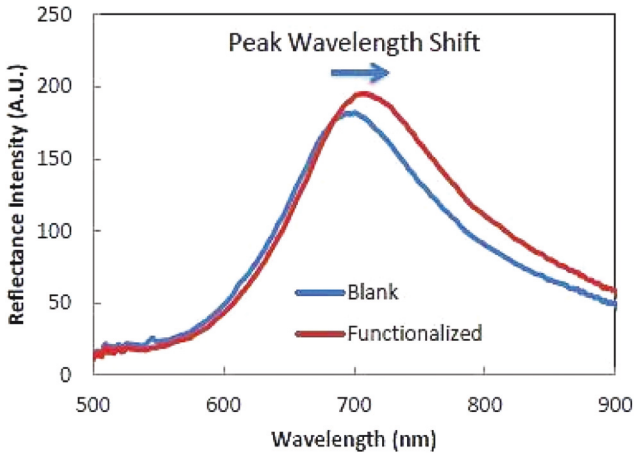

Fig. 3 Reflectance spectra of the ARC probe functionalization step.

data sets. Details of surface modification were analyzed according to the LSPR spectral shift. Assuming that the total peak shift came from increasing the organic layer thickness, the effective dielectric layer thickness could be calculated, hence the equivalent thickness change before and after the ARC DNA probe attachment can be obtained according to the relationship of the measured LSPR peak shift, SPR decay length, nanoprobe RI sensitivity, and dielectric environment, as reported previously.[25] From the measured bulk RI sensitivity of 227 nm RIU^{-1}, one could estimate the equivalent molecular thickness of the ARC probe DNA added to the Au nanodisk surface according to the equation:[30,31]

$$\Delta\lambda = m(n_{add} - n_{air})\left[\exp\left(-2d_{pre}/l_d\right)\right] \left[1 - \exp(-2d_{add}/l_d)\right]. \quad (2)$$

In eqn (2), $\Delta\lambda$ is defined as the SPR signal response (peak shift) after addition of the molecular layer to the preceding step modification, and m is the measured LSPR-FO probe sensitivity. d_{pre} is the effective thickness of the existing layer (using 0 nm for the clean interface), and l_d is the decay length of SP mode into the dielectric at the nanodisk array (two l_d values of 30 and 45 nm were used respectively for calculation according to the nanodisk dimension aspect[32]). The RI of DNA molecules was taken to be 1.5 (n_{add}) and that of air as 1.0 (n_{air}).

According to the average peak shift $\Delta\lambda$ of 8.3 nm, using eqn (2), the calculated equivalent thickness increases of the functionalization step were ~1.14 nm (l_d 30 nm) or ~1.72 nm (l_d 45 nm). We assumed that this increase came from ARC probe DNA molecular adsorption. The ARC probe DNA, a 20-base-pair ssDNA, was tethered to the Au surface by an Au–thiol bond and a fixed length, non-interacting, standard six-carbon (MC6) alkane spacer (~0.5 nm length) linker. The effective length of the ssDNA tethered to a surface would depend on the conformation of the probe DNA, surface properties, salt concentration, and the number of base pairs. Under the experimental conditions, the average stretched length of the ARC probe DNA was about 7.3 nm in water.[33] The ssDNA, however, has weak stiffness; it tends to curl on itself more, compared to its double-strand DNA (dsDNA) counterpart and thus decreases the achievable surface molecular density.[34] The coverage of probe DNA at the LSPR sensing area was estimated to be ~14.3% (l_d 30 nm) or ~21.5% (l_d 45 nm) based on the ratio of the calculated film thickness to the stretched DNA length.

Detection of target ARC DNA

Concentrations of ARC DNA from 1 fM to 100 μM were used for measurements by the ARC functionalized LSPR-FO nanoprobe. For each concentration, the reaction time was 10 min. Fig. 4 illustrates the reflectance spectra at different ARC target concentrations (Fig. 4a) and the peak shift as a function of the concentration (Fig. 4b). The quantity of binding can be obtained for each dilution by viewing the graph of average LSPR peak wavelength shifts of target binding.

The limit of detection (LOD) is the lowest concentration for identification of a wavelength shift. The average standard deviation of the experimental data for 3 tests was ±1.6 nm. A wave-

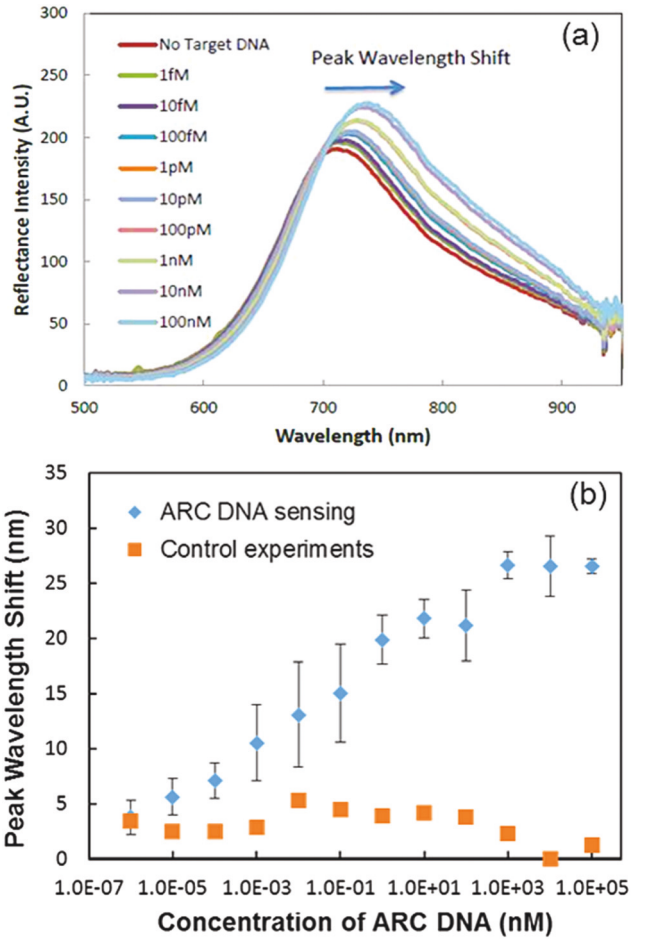

Fig. 4 (a) The representative reflectance spectra of the ARC probe DNA modified LSPR-FO tip in various ARC target DNA concentrations. (b) LSPR peak wavelength shift due to the specific binding of ARC target DNA to the ARC probe DNA on the Au nanodisk surfaces of the optical fiber end facet. The error bars represent the standard deviations calculated from three independent measurements.

length shift (~5 nm) triple the signal-noise ratio (S/N, *i.e.* the average standard deviation) can be used to determine the LOD of the fiber LSPR sensors. This corresponds to 10 fM of ARC ssDNA in water. Note that the volume of the sample for detection was 10 μL, which indicates the detectable LOD of ~60 000 pieces of ARC ssDNA target in the sample.

Control experiments

Control experiments were performed to assess non-specific binding to the ARC probe DNA functionalized LSPR-FO. For these experiments, another strand of 20 base pairs of DNA, NEG DNA, was used. The NEG DNA was designed so that it is unlikely to bind to the ARC DNA probe on the tip surfaces. Various concentrations of NEG DNA from 1 fM to 100 μM were used to test the response of the LSPR-FO functionalized for ARC DNA. From the peak shift value obtained in the NEG DNA solutions, there were insignificant and random changes in the peak wavelength shift, around the LOD level ($\lesssim$5 nm). This is because the sequences of the probe ARC DNA and NEG DNA were not matched; thus, in this situation, there was no appreciable DNA hybridization. This result suggests that the nanodisk array-based LSPR-FO devices, along with tailored surface functionalization with appropriate probe DNA receptors, can be used for detection of DNA with excellent sensitivity and specificity over a broad concentration range. Moreover, the LSPR-FO nanodisk probe can be reused with reproducible LSPR spectra (Fig. S2†) after cleaning with a "piranha" solution (a mixture of 30% H_2O_2 and 98% H_2SO_4 in a 1 : 3 volume ratio), indicating its excellent stability.

FDTD simulation and sensitivity

To understand the above experimental results, we used the FDTD method (Fig. 5a) to study the relationship between the wavelength shift and the thickness of the added bio-organic layer. Fig. 5(b and c) and S3 show that the red-shift presents with increasing thickness of the bio-organic layer. For the LSPR peak shift of ~8.6 nm, the thickness of the bio-organic layer added was 1 nm, which was consistent with the above experimental results. Moreover, in terms of increasing the bio-organic layer, the presence of a wavelength shift between the layer additions of 4 nm and 12 nm suggested that there is no saturation point in this FDTD model compared to the binding between probe DNA and target DNA in the experiment above. This is understandable due to the limited density of ARC ssDNA probes immobilized at the gold surface.

Furthermore, whether at the reflected surface or at the transmitted surface, the maximum electric field intensity of the 4 nm DNA/Au nanodot was 4 $(V\ m^{-1})^2$ higher than that of the 0 nm DNA/Au nanodot (Fig. 6), which has the same trend as the magnetic field distribution (near field, Fig. S4†). This can be attributed to the stronger collective oscillation of surface electrons in the model of the 4 nm DNA/Au nanodot than that of the model of the 0 nm organic layer Au nanodot when certain wavelengths of light shoot to the particle surface, since the electron density distribution in the metal is uneven with incident light at a specific wavelength.[4,35] Hence, in the model of the 4 nm DNA/Au nanodot, with Δt between transmitted light through the Au nanodot and reflected light from the bio-organic layer, the collective oscillation of the interface between the Au nanodot and the bio-organic layer will be stronger because of the coupled incident light.

Next, in the area of electron density below the average density, a local excess positive charge is formed. Meanwhile,

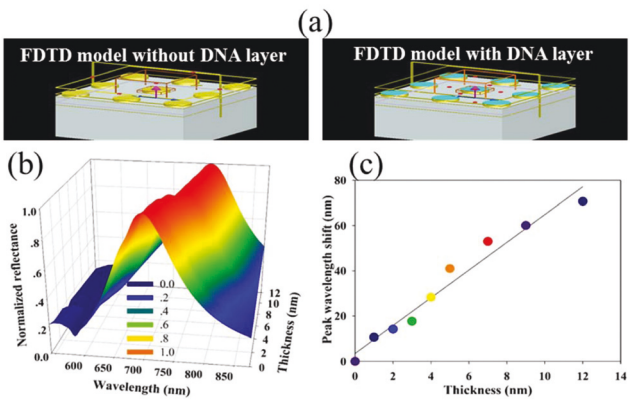

Fig. 5 (a) Scheme of FDTD simulation of 0 nm DNA/Au nanodot (left) and 4 nm DNA/Au nanodot (right). (b) The FDTD simulated reflectance spectra in various thicknesses of the DNA layer, where the spectra are normalized. (c) Simulation results of the peak wavelength shift *vs.* organic layer thickness at the gold nanodot surfaces.

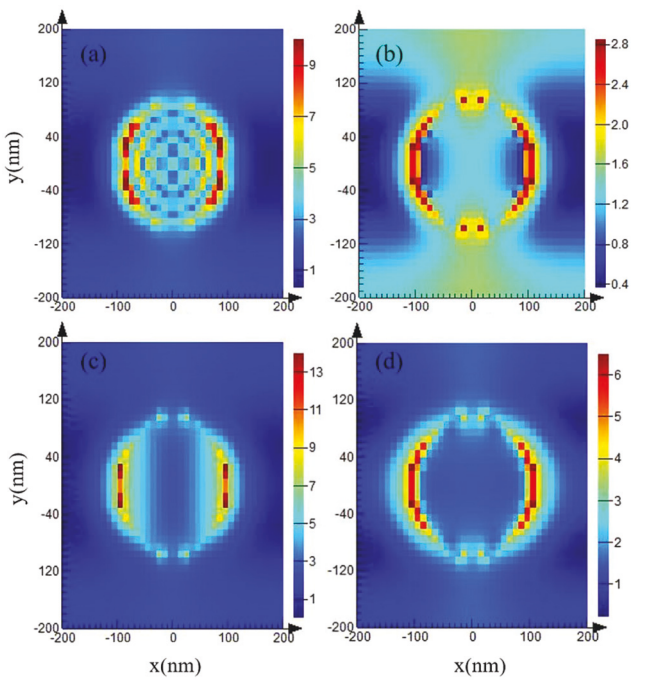

Fig. 6 FDTD calculated electric field distribution (near field) on the reflected and transmitted side: (a) reflected surface of 0 nm DNA/Au nanodot; (b) transmitted surface of 0 nm DNA/Au nanodot; (c) reflected surface of 4 nm DNA/Au nanodot; (d) transmitted surface of 4 nm DNA/Au nanodot. Note the unit of electric field intensity (E^2) is $(V\ m^{-1})^2$.

the nearby electrons will be drawn into the field resulting from the gravitational influence of Kunlun.[36] Then, due to the electrons' inertia, many negative electrons will gather in that region. However, the repulsion between the electrons will make them leave the area again, which results in the oscillation of the valence electrons relative to the background of positive charge density. Consequently, the intensity of the field distribution and the LSPR performance will be higher with stronger oscillations. The distribution of the electric field can be evaluated by the following equations:[36]

$$E_{\text{in}} = \frac{3\varepsilon_{\text{m}}}{\varepsilon + 2\varepsilon_{\text{m}}} E_0 \quad (3)$$

$$E_{\text{out}} = E_0 + \frac{3n(np) - p}{4\pi\varepsilon_0\varepsilon_{\text{m}}} \frac{1}{r^3} \quad (4)$$

where ε is the dielectric function and p is the dipole moment. Many applications of metal nanoparticles in optical devices and sensors rely on this field-enhancement at the plasmon resonance at both the internal and dipolar fields.[36,37] Hence, the response of the DNA hybridization is enhanced, resulting in the high sensitivity of the LSPR-FO nanoprobe for detection.

Conclusions

In conclusion, a miniaturized, robust, localized surface plasmon resonance (LSPR) coupled fiber-optic (FO) nanoprobe was developed for detection of DNA hybridization and measurement of DNA concentrations. The LSPR-FO system potentially provides a highly integrated and portable solution for a label-free point-of-care detection from small sample volumes (~μL). The FO nanoprobe, created by constructing metallic nanostructured disk arrays at the end facets of optical fibers, demonstrated excellent sensitivity, stability, and reusability. The lowest LOD for a DNA of 20 bases in buffer solution was 10 fM and was highly selective. The FDTD simulation and modeling of the optical response upon the DNA functionalization at the nanoprobe and DNA hybridization for detection provided insight into the underlying LSPR phenomena at the nanodisk structures and understanding of sensing scenario, offering a direction to optimize the nanostructure for enhanced plasmon resonance. The experimental and modeling results demonstrate the advances of the LSPR-FO nanoprobe device as a compact and low-cost biosensor for highly sensitive, label-free detection of short strand DNA.

Acknowledgements

ZZ and JW have been partially supported by a US NSF grant (Grant # 1511194). SK and YL acknowledge financial support from UAH and NSF EPSCoR (Grant 34-21530-200-76190). UM has been partially supported by the National Institutes of Health grants P20CA192973 and U54 CA118948. The authors thank Dr Donald Hill for his critical review of the manuscript.

Notes and references

1 J.-K. Chen, G.-Y. Zhou, C.-J. Chang and C.-C. Cheng, *Sens. Actuators, B*, 2014, **194**, 10–18.
2 J. N. Anker, W. P. Hall, O. Lyandres, N. C. Shah, J. Zhao and R. P. Van Duyne, *Nat. Mater.*, 2008, **7**, 442–453.
3 J. Cao, T. Sun and K. T. V. Grattan, *Sens. Actuators, B*, 2014, **195**, 332–351.
4 J. Homola, S. S. Yee and G. Gauglitz, *Sens. Actuators, B*, 1999, **54**, 3–15.
5 C. R. Yonzon, E. Jeoungf, S. L. Zou, G. C. Schatz, M. Mrksich and R. P. Van Duyne, *J. Am. Chem. Soc.*, 2004, **126**, 12669–12676.
6 J. Homola, *Chem. Rev.*, 2008, **108**, 462–493.
7 K. M. Mayer and J. H. Hafner, *Chem. Rev.*, 2011, **111**, 3828–3857.
8 K. A. Willets and R. P. Van Duyne, *Annu. Rev. Phys. Chem.*, 2007, **58**, 267–297.
9 E. Cubukcu, N. F. Yu, E. J. Smythe, L. Diehl, K. B. Crozier and F. Capasso, *IEEE J. Sel. Top. Quantum Electron.*, 2008, **14**, 1448–1461.
10 H. C. Jeon, C.-J. Heo, S. Y. Lee and S.-M. Yang, *Adv. Funct. Mater.*, 2012, **22**, 4268–4274.
11 E. Petryayeva and U. J. Krull, *Anal. Chim. Acta*, 2011, **706**, 8–24.
12 J. Zhao, X. Zhang, C. R. Yonzon, A. J. Haes and R. P. Van Duyne, *Nanomedicine*, 2006, **1**, 219–228.
13 H.-H. Jeong, N. Erdene, J.-H. Park, D.-H. Jeong, H.-Y. Lee and S.-K. Lee, *Biosens. Bioelectron.*, 2013, **39**, 346–351.
14 W. Shi, Y. Sahoo, M. T. Swihart and P. N. Prasad, *Langmuir*, 2005, **21**, 1610–1617.
15 P. Alonso-Gonzalez, P. Albella, F. Golmar, L. Arzubiaga, F. Casanova, L. E. Hueso, J. Aizpurua and R. Hillenbrand, *Opt. Express*, 2013, **21**, 1270–1280.
16 O. L. Muskens, V. Giannini, J. A. Sanchez-Gil and J. Gomez Rivas, *Opt. Express*, 2007, **15**, 17736–17746.
17 F. Hao, C. L. Nehl, J. H. Hafner and P. Nordlander, *Nano Lett.*, 2007, **7**, 729–732.
18 J. Fischer, N. Vogel, R. Mohammadi, H. J. Butt, K. Landfester, C. K. Weiss and M. Kreiter, *Nanoscale*, 2011, **3**, 4788–4797.
19 A. Ricciardi, A. Crescitelli, P. Vaiano, G. Quero, M. Consales, M. Pisco, E. Esposito and A. Cusano, *Analyst*, 2015, **140**, 8068–8079.
20 C. Caucheteur, T. Guo and J. Albert, *Anal. Bioanal. Chem.*, 2015, **407**, 3883–3897.
21 X.-d. Wang and O. S. Wolfbeis, *Anal. Chem.*, 2016, **88**, 203–227.
22 Y. Lin, J. Guo and R. G. Lindquist, *Opt. Express*, 2009, **17**, 17849–17854.
23 Y. Lin, Y. Zou, Y. Mo, J. Guo and R. G. Lindquist, *Sensors*, 2010, **10**, 9397–9406.
24 Y. B. Lin, Y. Zou and R. G. Lindquist, *Biomed. Opt. Express*, 2011, **2**, 478–484.
25 M. Sanders, Y. Lin, J. Wei, T. Bono and R. G. Lindquist, *Biosens. Bioelectron.*, 2014, **61**, 95–101.

26 J. Boateng, J. Peek, R. Zahorchak and K. Chittur, *Anal. Biochem.*, 2012, **430**, 39–44.
27 J. Boateng, R. Zahorchak, J. Peek and K. Chittur, *Anal. Biochem.*, 2013, **435**, 60–67.
28 Z. Zeng, Y. Liu and J. Wei, *TrAC, Trends Anal. Chem.*, 2016, **75**, 162–173.
29 E. D. Palik, in *Handbook of Optical Constants of Solids*, Academic Press, Burlington, 1997.
30 L. S. Jung, C. T. Campbell, T. M. Chinowsky, M. N. Mar and S. S. Yee, *Langmuir*, 1998, **14**, 5636–5648.
31 S. Haemers, G. J. M. Koper, M. C. van der Leeden and G. Frens, *Langmuir*, 2002, **18**, 2069–2074.
32 S. Chen, M. Svedendahl, M. Käll, L. Gunnarsson and A. Dmitriev, *Nanotechnology*, 2009, **20**, 434015.
33 K. K. Kunze and R. R. Netz, *Phys. Rev. Lett.*, 2000, **85**, 4389–4392.
34 H. P. Erickson, *Biol. Proced. Online*, 2009, **11**, 32–51.
35 Z. Zeng, M. N. Mendis, D. H. Waldeck and J. Wei, *RSC Adv.*, 2016, **6**, 17196–17203.
36 S. A. Maier, *Plasmonics: Fundamentals and Applications*, Springer US, 1st edn, 2007.
37 S. K. Ghosh, S. Nath, S. Kundu, K. Esumi and T. Pal, *J. Phys. Chem. B*, 2004, **108**, 13963–13971.